ISSN 0884-5913, Kinematics and Physics of Celestial Bodies, 2021, Vol. 37, No. 6, pp. 300–309. © Allerton Press, Inc., 2021.
Russian Text © The Author(s), 2021, published in Kinematika i Fizika Nebesnykh Tel, 2021, Vol. 37, No. 6, pp. 49–61.

SOLAR PHYSICS

The Fe IX Line at 17.1 nm in the Radiation Spectrum of Slow Magneto-Acoustic Waves Propagating in the Solar Corona

S. G. Mamedov[a, *], Z. F. Aliyeva[b], and K. I. Alisheva[a, b]

[a] *Shamakhy Astrophysical Observatory named after Nasraddin Tusi, Azerbaijan National Academy of Sciences, Y. Mammadaliyev settlement, Shamakhy raion, AZ-5626 Azerbaijan*

[b] *Baku State University, Baku, AZ1148 Azerbaijan*

**e-mail: sabirmamedov@mail.ru*

Received June 10, 2021; revised July 29, 2021; accepted August 19, 2021

Abstract—Profiles of the Fe IX line at a wavelength of $\lambda = 17.1$ nm in the radiation spectrum of slow magneto-acoustic waves, propagating in coronal loops, are calculated under conditions of an optically thin layer and a constant density. The parameter values used in calculations of the line profiles are as follows: the amplitude of the velocity of particles' displacements in a wave $v_0 = 10$ km/s, the width of the coronal loop is 2000 and 5000 km, the wavelength $\Lambda = 20000$ km and 50000 km, and the value of the Doppler width $\Delta\lambda_d = 1$ pm; the values for the angle of view and the wave phases were varied. The true value of the energy flux density is 622 erg/cm^{2}s. The values of the energy flux density obtained in calculations strongly depend on the angle of view θ and the wave phase: they range from 0 and, when the values of θ are large, to 2000 erg/cm^{2}s. The values of the Doppler velocities v_d and the velocities of nonthermal motions v_{nt} take maximal values of ~12 km/s at small angles θ and almost vanish at large angles θ. When the angle of view is small ($\theta < 30°$), a weak blue asymmetry is noticeable. When the angle of view is large ($\theta > 30°$), the asymmetry is almost invisible.

Keywords: solar corona, MHD waves, slow magneto-acoustic waves

DOI: 10.3103/S0884591321060064

INTRODUCTION

The studies of magnetohydrodynamic (MHD) waves in coronal structures is an important field in coronal seismology. These waves may play a significant part in heating the corona, and, moreover, the analysis of these waves may serve as a basis for investigating the physical structure of the solar corona.

Slow magneto-acoustic waves are considered to be one of the mechanisms that can warm the solar corona up: these waves are generated in the photosphere as a *p*-mode, penetrate into the corona without being reflected, and decay due to the thermal conductivity mechanism, which results in warming the corona.

Before the 1990s, MHD waves in the corona were studied mainly theoretically. In the early 2000s, intensive extraterrestrial observations of these waves in the UV range of the corona's spectrum started. These issues are described at length in reviews [1, 5–7, 10, 22].

Below, we calculate a profile of the Fe IX line at a wavelength of $\lambda = 17.1$ nm in the spectrum of slow magneto-acoustic waves propagating in coronal loops. Observations of these waves at this wavelength are rather frequent [7].

The physical parameters of slow magneto-acoustic waves obtained in observations are as follows: the propagation velocity is 25–200 km/s, the amplitude of oscillations in intensity is 0.7–14.6%, the oscillation period is 145–550 s [7], and the energy flux density ranges from 313 to (6×10^6) erg/cm^{2}s [13, 20]. It is of interest that the Doppler shift velocities observed in the chromosphere and the corona are almost an order of magnitude smaller than the nonthermal velocities determined from the Doppler widths [26].

MHD waves, which are generated in photospheric layers of the solar atmosphere, are considered to be one of the main mechanisms of heating the solar corona. The values of the parameters from which the energy flux of the waves is calculated are obtained from observations. The consideration is focused on the Alfvén and slow magneto-acoustic waves propagating in coronal structures. The studies of this problem show that the Alfvén waves have a greater potential in heating the corona, while slow magneto-acoustic waves do not have much energy that would be sufficient for warming the corona up.

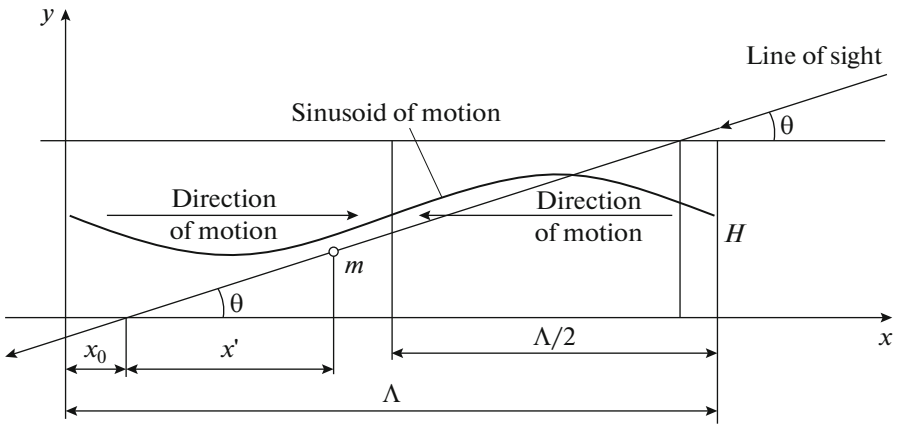

Fig. 1. Scheme of propagation of a slow magneto-acoustic wave inside a coronal loop; H is the loop diameter, Λ is the sound wavelength, θ is the angle between the line of sight and the loop axis direction, x_0 is the distance from the zero phase point of the wave (this point is also the coordinate system origin) to the point of intersection of the line of sight and the X-axis (which characterizes the phase), x' is the distance along the X-axis from the point of intersection of the line of sight and the X-axis to the volume element considered, and l is the distance along the line of sight from the point of intersection of the line of sight and the X-axis to the volume element considered.

Hence, it is of interest to calculate a profile of the line in the radiation spectrum of a magneto-acoustic wave for different physical parameters, to estimate the energy flux, and to compare them with those observed. We calculated profiles of the Fe IX line at a wavelength of $\lambda = 17.1$ nm, which is often observed in the spectrum of slow magneto-acoustic waves; the calculations were performed for a case of an optically thin layer and a constant density.

EXPRESSION TO CALCULATE A SPECTRAL LINE PROFILE

Our task is to calculate a profile of the line in the radiation released from a coronal loop along the line of sight making the angle θ with the loop axis.

To our knowledge based on literature sources, the profiles of spectral lines in the spectrum of slow magneto-acoustic waves propagating in coronal structures have not been calculated so far.

We will assume here that a coronal loop is optically thin and the density within a wave is constant (in the future, we plan to consider a case of varying density).

The profile of radiation released by a volume element along the line of sight is of the Doppler type, and its width $\Delta\lambda_d$ is assumed to be constant along the line of sight.

Figure 1 schematically shows how a slow magneto-acoustic wave propagates inside a coronal loop (its diameter is H) along the X-axis of the coordinate system XY, which originates from the zero phase of the considered wave. The X- and Y-axes are directed along the loop axis and perpendicular to it, respectively. See the figure caption for details.

The amount of radiation released by a volume element ($dl \times 1$ cm^2) at a distance l from the surface of a coronal loop at a wavelength, which is at a distance $\Delta\lambda$ from the line center, is

$$di(\Delta\lambda) = i_0 \exp\left[-\left(\frac{\Delta\lambda - \frac{v(l)}{c}\lambda}{\Delta\lambda_d}\right)^2\right] dl. \quad (1)$$

Here, i_0 is the intensity in the center of the profile of the volume element chosen, which is assumed to be constant along the line of sight, $v(l)$ is the velocity of particles in a wave at a distance l, and c is the velocity of light. The intensity of the radiation from the whole line of sight L at a distance $\Delta\lambda$ from the line center will then be

$$I(\Delta\lambda) = i_0 \int_0^L \exp\left[-\left(\frac{\Delta\lambda - \left(\frac{v(l)}{c}\lambda\right)}{\Delta\lambda_d}\right)^2\right] dl. \quad (2)$$

We now should find $v(l)$. In an acoustic wave, particles move along the wave propagation direction according to the sine law (as is seen in Fig. 1, $x = x_0 + x'$)

$$v(x) = v_0 \sin\left(\frac{2\pi x}{\Lambda}\right).$$

For the lines of sight that pass through the point x_0 (the quantity x_0 approximately characterizes the wave phase), it is convenient to use the following expression, where x is substituted by $x_0 + x'$ and the quantity x' is a variable:

$$v(x') = v_0 \sin\left(\frac{2\pi(x_0 + x')}{\Lambda}\right). \quad (3)$$

Here, v_0 is the amplitude of oscillation velocities of particles and Λ is the wavelength of a propagating slow magneto-acoustic wave.

It is clear that the projection of the amplitude of velocities of particles onto the line of sight will be

$$v_{0L} = v_0 \cos\theta. \quad (4)$$

Then,

$$x' = l\cos\theta. \quad (5)$$

and

$$v(l) = v_0 \cos\theta \sin\left[\frac{2\pi(x_0 + l\cos\theta)}{\Lambda}\right]. \quad (6)$$

By introducing expression (6) into Eq. (2), we derive a final formula to calculate the spectral line profile:

$$I(\Delta\lambda) = i_0 \int_0^L \exp\left[-\left(\frac{\Delta\lambda - v_0 \cos\theta \sin\left[\frac{2\pi(x_0 + l\cos\theta)}{\Lambda}\right]\frac{\lambda}{c}}{\Delta\lambda_d}\right)^2\right] dl. \quad (7)$$

As can be seen from Fig. 1, the line of sight passes through the medium moving in opposite directions in the wave; consequently, to calculate the line profile, this expression was divided into two integrals for both sections of the motion in the following way:

$$I(\Delta\lambda) = i_0 \int_0^{l_1} \exp\left[-\left(\frac{\Delta\lambda - v_0 \cos\theta \sin\left[\frac{2\pi(x_0 + l\cos\theta)}{\Lambda}\right]\frac{\lambda}{c}}{\Delta\lambda_d}\right)^2\right] dl$$
$$+ i_0 \int_{l_1}^{l_2} \exp\left[-\left(\frac{\Delta\lambda + v_0 \cos\theta \sin\left[\frac{2\pi(x_0 + l\cos\theta)}{\Lambda}\right]\frac{\lambda}{c}}{\Delta\lambda_d}\right)^2\right] dl. \quad (8)$$

$$l_1 = \left(\frac{\Lambda}{2} - x_0\right)\sec\theta,$$

$$l_2 = \left[H - \left(\frac{\Lambda}{2} - x_0\right)\tan\theta\right]\mathrm{cosec}\theta.$$

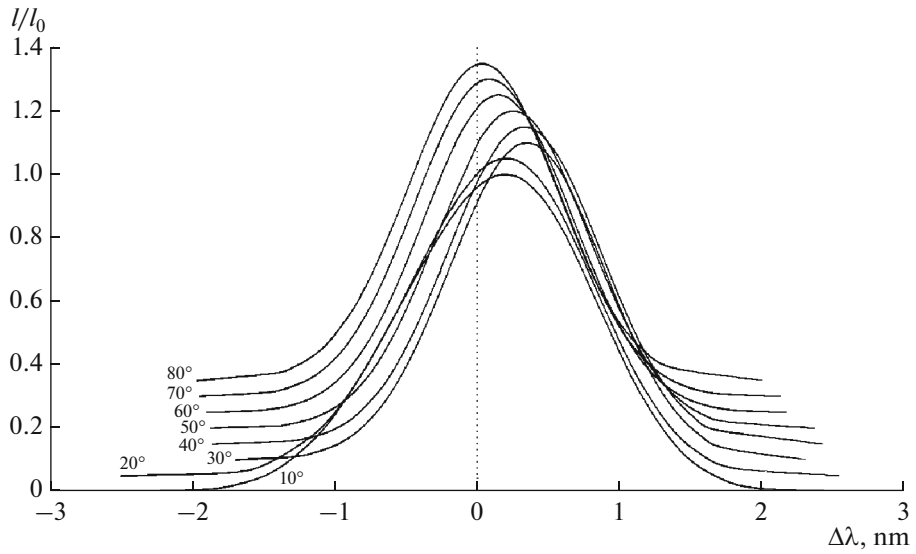

Fig. 2. Profiles of the Fe IX line at a wavelength of λ = 17.1 nm calculated for different angles of the line of sight θ and the wavelength Λ = 20000 km. The profiles are normalized to the intensity at the center and vertically shifted relative to each other by 0.05.

With the expression

$$v_d = \frac{\int_0^L v(l)dl}{L},$$

we find the Doppler shift as

$$v_{sh} = \frac{v_0\Lambda}{2\pi L}\left[-\cos\left(\frac{2\pi x_0}{\Lambda} + \frac{2\pi L\cos\theta}{\Lambda}\right) + \cos\frac{2\pi x_0}{\Lambda}\right]. \quad (9)$$

The calculations were performed for the Fe IX line at a wavelength of λ = 17.1 nm, which is rather frequently used in observations of slow magneto-acoustic waves. The following parameters were used in calculations: v_0 = 10 km/s; Λ = 20000 and 50000 km [8, 16]; H = 2000 and 5000 km; $\Delta\lambda_d$ = 0.01, which corresponds to the temperature $T = 10^6$; and $L = H/\cos t\theta$, where the angle between the line of sight and the wave propagation direction takes the values θ = 10°, 20°, 30°, 40°, 50°, 60°, 70°, and 80°. In Fig. 2, we present examples of the profiles calculated. From modeling a profile of the considered spectral line, we may determine how sensitive the quantities of the energy flux and the nonthermal and Doppler shifts are to variations in different parameters. The diagrams resulting from the calculations are shown in the corresponding figures below.

RESULTS

Velocities of the Doppler Shifts and Nonthermal Motions

Figure 3 presents the velocities of Doppler shifts v_d and nonthermal motions v_{nt} in dependence on the angle of inclination θ for the wavelengths Λ = 20 000 and 50 000 km and the loop diameter H = 5000 km. In Fig. 4, the values of v_d and v_{nt} are shown for the wavelength Λ = 50000 km and the loop diameters H = 2000 and 5000 km. In Fig. 5, the velocities v_d and v_{nt} are shown in dependence on the angle of sight θ for different values of the phase x_0 and the parameters H and Λ.

The values of the Doppler shift velocities v_d obtained from different observations are conflicting: v_d = 3 [26], 1.8–3.7 [19], 0.2–1.2 [14], 0.3–0.7 [28], 1.3–1.6 [30], 0.3–2.5 [18], and 3 km/s [3]. For standing waves, the values of the Doppler velocities are significantly higher: v_d = 18 [32], 200 [4], and 191 km/s [31]. According to the data of several studies described in [26], the values of the nonthermal velocities (v_{nt} = 23 km/s) are almost an order of magnitude higher than the Doppler shift velocities. Based on the results of our calculations, it is difficult to explain the data presented in [26].

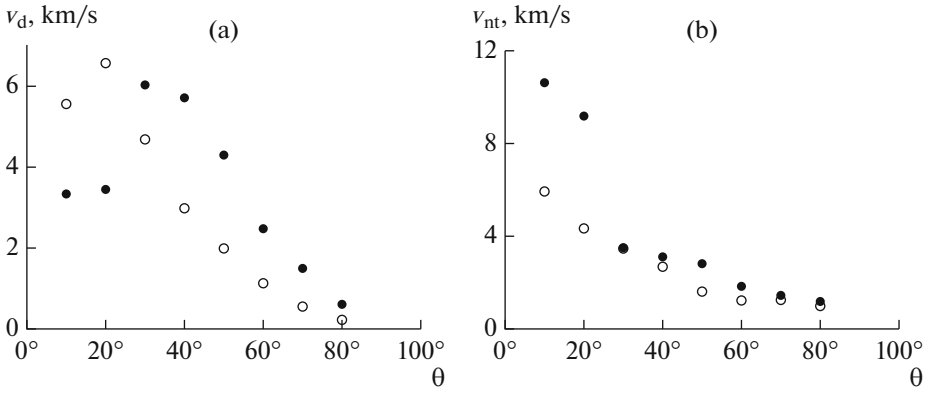

Fig. 3. Velocities of Doppler shifts v_d and nonthermal motions v_{nt} in dependence on the angle of inclination θ for H = 5000 km, x_0 = 500, and different values of the wavelengths Λ = 20000 km (dots) and 50000 km (open circles).

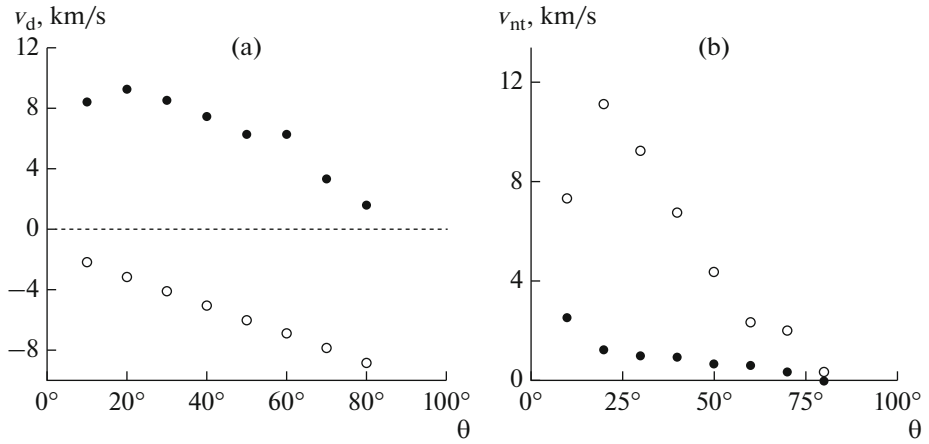

Fig. 4. Velocities of Doppler shifts v_d and nonthermal motions v_{nt} in dependence on the angle of inclination θ for Λ = 50000 km, x_0 = 10 000, and different values of the loop diameters H = 2000 km (dots) and 5000 km (open circles).

As regards the values of the nonthermal velocities obtained from observations, we note that there have not been many attempts to determine v_{nt} in the radiation spectrum of slow magneto-acoustic waves. For example, from observations of many coronal lines of an active region, the nonthermal velocities were estimated at 17 and 10 km/s, respectively, in [2] and [25]. From observations in the 17.1-nm line, the values 7.5 and 3 km/s were obtained in [9] and [23], respectively. According to observations [27], which were carried out in the 530.3-nm line of Fe XIV in the spectrum of slow waves, the velocities of Doppler shifts and nonthermal motions are 0.3 and 10–20 km/s, respectively. As we see, these values are within the limits we found in calculations.

In [15], the Doppler shift up to 300 km/s was detected in coronal loops. The authors of that paper explain this value by motions in slow magneto-acoustic waves. However, those observations were carried out at the solar limb, i.e., perpendicularly to a tube of the loop. Consequently, since a slow acoustic wave propagates along a tube and particles within it move along the propagation direction, the line of observations was perpendicular to the motions in the wave, due to which the observed motions cannot be motions in a slow magneto-acoustic wave. Most likely, the observed motions are motions in a bending wave. The estimate obtained in [24] is v_d = 84 km/s, and the observed wave is considered to be a slow magneto-acoustic wave. However, at the moment of observations, there was a phase shift of 90° between the changes in the density n_1 and the velocity of motions v_1 in a wave. Since the change in the density means the change in the intensity, we may conclude that the observed wave was a standing slow magneto-acoustic wave.

Figure 5 shows the velocities of nonthermal motions v_{nt} and Doppler shifts υ_d in dependence on the angle of view θ for different values of the wave phase x_0, the wavelength Λ, and the coronal loop width H. As is seen, the velocity values change from 12 km/s to almost zero under small and large values of the angle of view, respectively. The values of the Doppler shifts under large angles of view are close to those

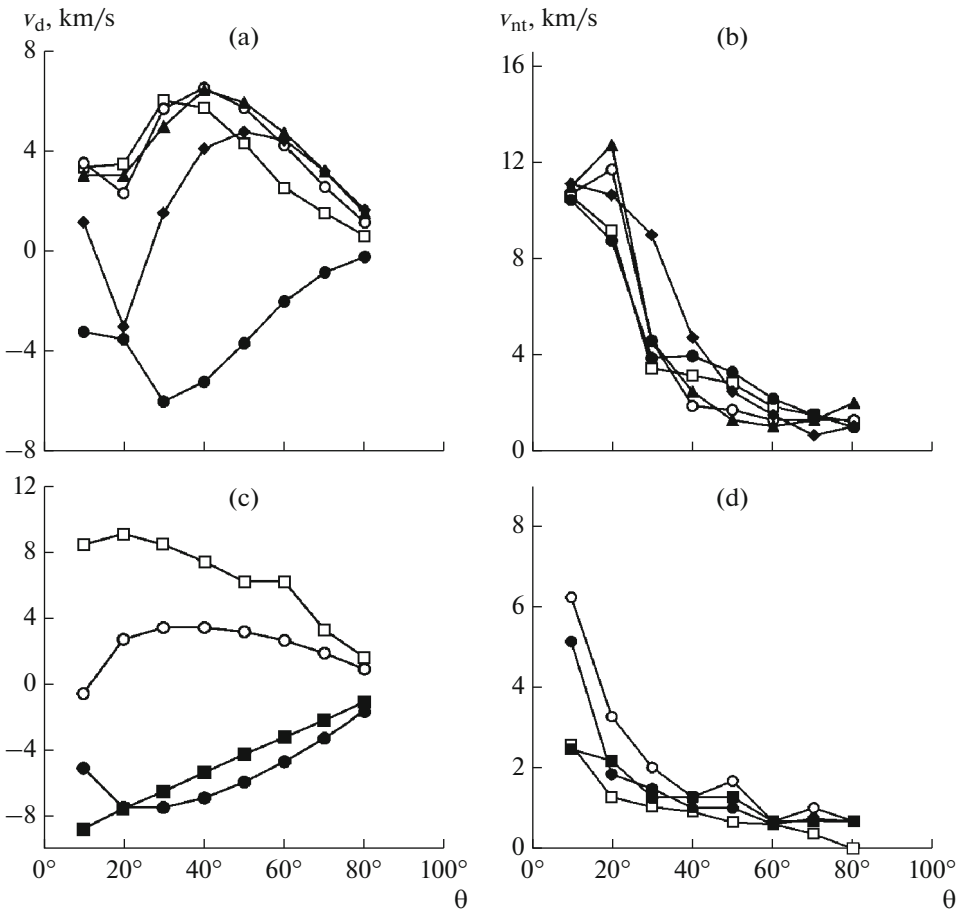

Fig. 5. Velocities (a, c) v_d and (b, d) v_{nt} in dependence on the angle of vision θ for different values of x_0. In (a) and (b), $H = 5000$ km and $\Lambda = 20000$ km, while $x_0 = 500$ (open squares), 2000 (open circles), 3000 (triangles), 5000 (diamonds), and 10000 (filled circles). In (c) and (d), $H = 2000$ km and $\Lambda = 50000$, while $x_0 = 10000$ (open squares), 20000 (open circles), 30000 (filled squares), and 40000 (filled circles).

observed; however, when the angles of view are small, the majority of calculated values substantially exceed the observed ones. Apparently, this can be explained by the fact that the actual amplitude of the velocities at these wavelengths is somewhat smaller than 10 km/s. We also note that, as is seen from Fig. 5, the velocity values depend on the loop width and the wavelength.

Energy Flux Density

In Fig. 6, we show the energy flux density F in dependence on the velocities of Doppler shifts υ_d and nonthermal motions v_{nt}, the values of which were obtained for the Doppler width at $H = 5000$ km, $\Lambda = 50000$ km, and $x_0 = 500$. As is seen, with increasing the velocities, the energy flux density grows, which is natural, while the increase in the angle of view θ to 100° results in decreasing the energy flux density. In Fig. 7, the energy flux density and the velocities are shown in dependence on the phase at $H = 5000$ km, $\Lambda = 20000$ km, and $\theta = 10°$.

In Fig. 8, we show the calculated values of the energy flux densities F_d and F_{nt} in dependence on the velocities of Doppler shifts v_d and nonthermal motions v_{nt}, respectively, which were obtained from the Doppler widths. In calculations, different values for the loop width, $H = 2000$ and 5000 km, and the wavelength, $\Lambda = 20000$ and 50000 km, were used. The flux densities were found according to the expression

$$F = \frac{1}{2}\rho v^2 v_{ph}.$$

Here, ρ is the density, v^2 is the mean square velocity of motions in a wave, and v_{ph} is the phase velocity of a wave.

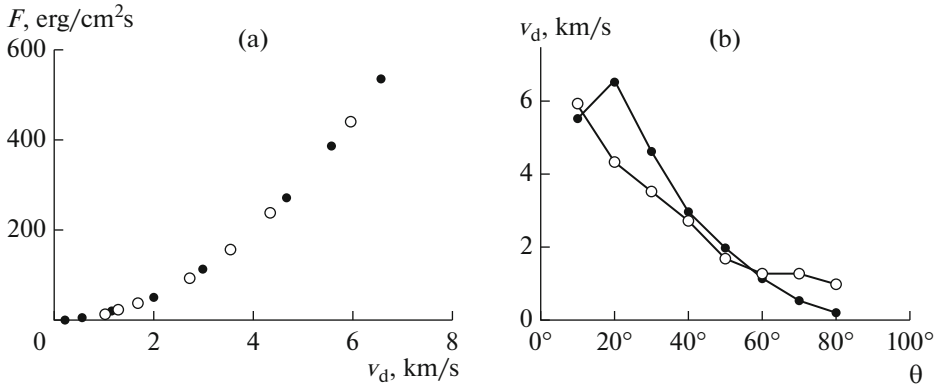

Fig. 6. (a) Energy flux densities F_d (dots) and F_{nt} (open circles) in dependence on the velocities of Doppler shifts v_d and nonthermal motions v_{nt}, respectively, which were obtained from the (in panel (b), dots and open circles, respectively) Doppler shifts for the following values of the parameters: $H = 5000$ km, $\Lambda = 50000$ km, and $x_0 = 500$.

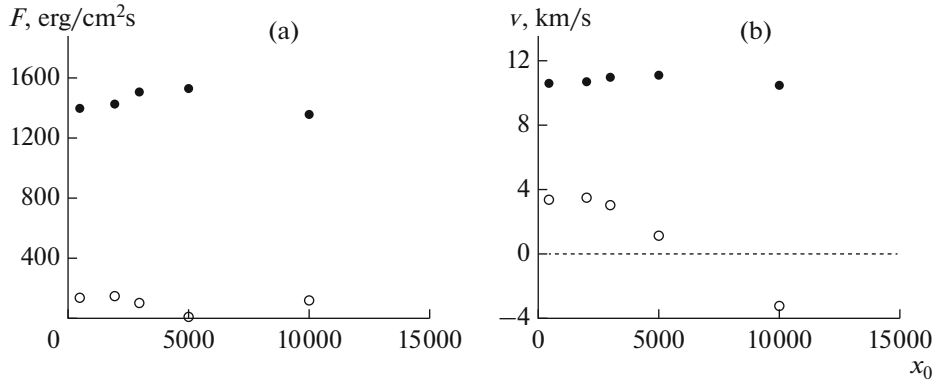

Fig. 7. (a) Energy flux densities F_d (dots) and F_{nt} (open circles) and the (b) velocities v_d (dots) and v_{nt} (open circles) in dependence on the phase x_0 for the following values of the parameters: $H = 5000$ km, $\Lambda = 20000$ km, and $\theta = 10°$.

As is seen from the diagrams, when $H = 5000$ km and $\Lambda = 20000$ km, the maximum in F_{nt} is almost four times higher than the maximum in F_d: 2000 vs. 550 erg/cm²s. However, when $H = 2000$ km and $\Lambda = 50000$ km, the situation is opposite: the maximum in F_d is almost two times as large as the maximum in F_{nt}: 1000 vs. 500 erg/cm²s. This result demonstrates that the flux values depend, in no small measure, on the loop width and the length of a slow acoustic wave propagating.

The flux values were calculated for different values of the wave phase. It is also seen from Fig. 8 how strongly the energy flux depends on the wave phase. The flux values change from 2000 erg/cm²s to almost zero at small and high values of the angle of view, respectively. We note that the values at low angles of view are close to those observed [7, 10].

The smallest values for the velocities of the Doppler shifts and nonthermal motions are 1 km/s and smaller; at the same time, the energy flux values are approximately 10 erg/cm²s and less. This means that, depending on the angle of view θ and the wave phase, the measured values of the energy flux should differ by almost two orders of magnitude and more. However, the amount of the energy that flows along a tube does not change! This amazing result may explain the considerably varying values for the energy flux of slow magneto-acoustic waves obtained by different researchers from observations [17]. A true value of the energy flux calculated by the expression

$$F = \frac{1}{4}\rho v_a^2 v_{ph}$$

under a specified value of the velocity amplitude in a wave $v_a = 10$ km/s is 622.5 erg/cm²s. An interesting result is that the values of the calculated (observed) energy flux may be both substantially smaller and substantially larger than the true value: they almost vanish at small values of θ.

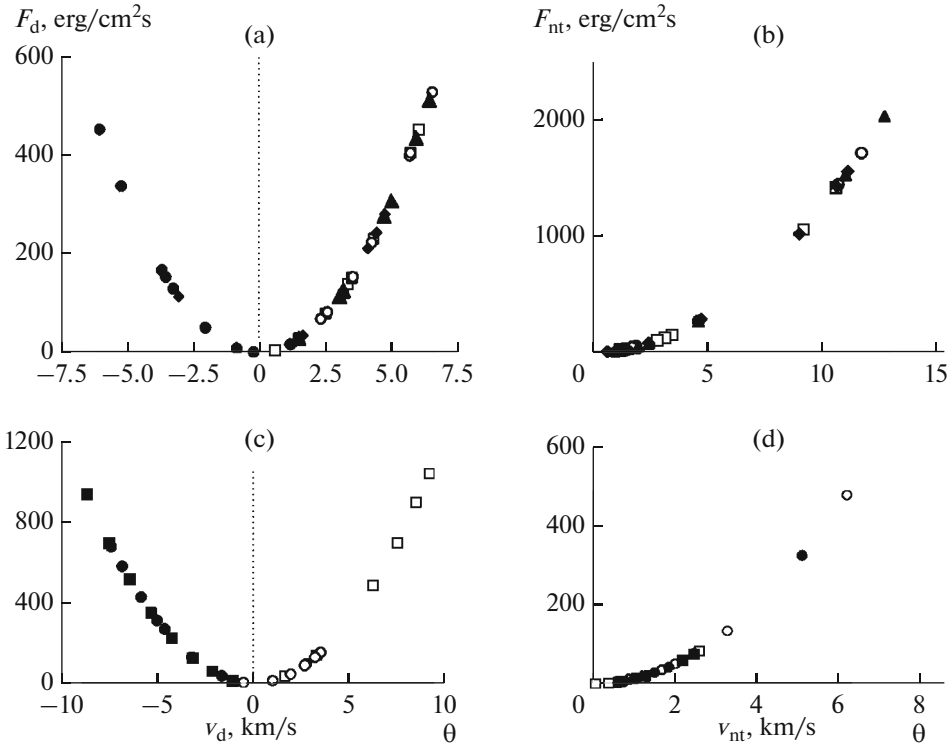

Fig. 8. Energy flux densities F_d and F_{nt} that were obtained from the Doppler widths in dependence on the velocities of Doppler shifts v_d and nonthermal motions v_{nt}, respectively. In (a, b), $H = 5000$ km and $\Lambda = 20000$ km, while $x_0 = 500$ (open squares), 2000 (open circles), 3000 (triangles), 5000 (diamonds), and 10 000 (filled circles). In (c, d), $H = 2000$ km and $\Lambda = 50000$, while $x_0 = 10000$ (open squares), 20000 (open circles), 30000 (filles squares), and 40 000 (filled circles).

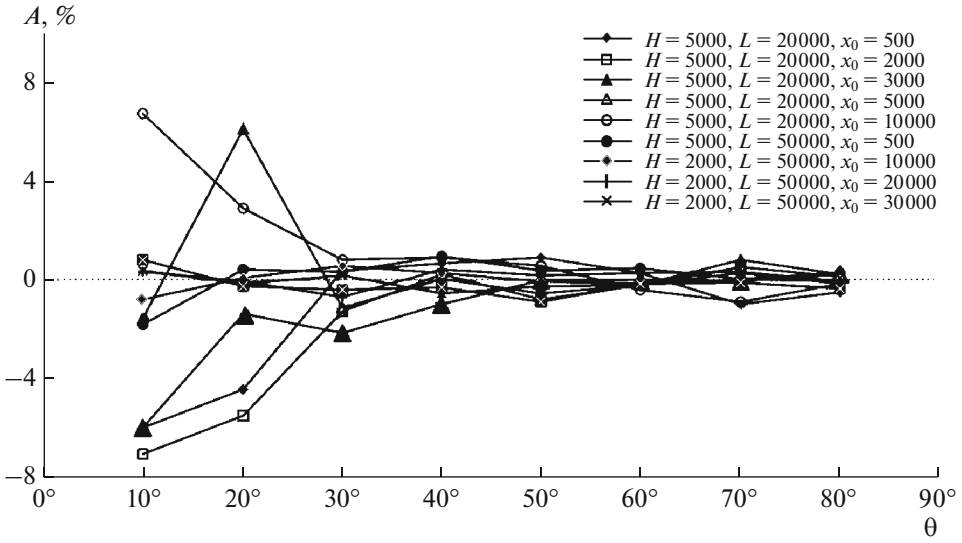

Fig. 9. Asymmetry A in dependence on the angle of view θ.

Asymmetry

To analyze the asymmetry in the lines of radiation of a magneto-acoustic wave, the areas enclosed by the profile within some wavelength intervals at the same distances from the line center are used. The line asymmetry is estimated by the expression $(R - B)/(R + B)$, where R and B are the areas on the red and blue sides from the line center, respectively. This makes it possible to reveal the mass flow that may cause the asymmetry [29].

We determined the *RB*-asymmetry from the entire blue and red wings, because, in our case, the asymmetry is generated by motions in the wave itself.

In almost all of the studies dealing with determining the cause of asymmetry in spectral lines, the authors come to the conclusion that the observed asymmetry is mainly "blue," which is produced by the upwelling plasma flow with velocities of 50–150 km/s [12, 21, 29]. In [21], the upwelling mass flow is identified with the type II spicules. In [11], the asymmetry is explained by a quasi-periodic motion of the upwelling mass flow, which is superimposed on a magneto-acoustic wave.

The asymmetry values determined here for all phases and wavelengths are presented in Fig. 9. As is seen, when the angle of view is small ($\theta < 30°$), a weak blue asymmetry is distinguishable. When the angle of view $\theta > 30°$, the asymmetry is almost unnoticeable. It can be said that motions in the wave itself produce no asymmetry in the spectral line profile. This is confirmed by the conclusion commonly made from many observations that the asymmetry is actually caused by the upwelling flow of matter, the radiation profile of which is superimposed on the radiation profile of a slow magneto-acoustic wave.

REFERENCES

1. M. J. Aschwanden, *Physics of the Solar Corona — An Introduction*, 1st ed. (Praxis, Chichester, 2004).
2. D. H. Brooks and H. P. Warren, "Measurements of non-thermal line widths in solar active regions," Astrophys. J. **820**, 63 (2016).
3. E. C. Bruner, "Dynamics of the solar transition zone," Astrophys. J. **226**, 1140–1146 (1978).
4. W. Surdt, T. J. Wang, D. E. Innes, S. K. Solanki, I. E. Damasch, B. Kliem, and L. Ofman, "Doppler oscillations in hot coronal loops," in *Solar Variability: From Core to Outer Frontiers: Proc. 10th Eur. Solar Physics Meeting, Prague, Czech Republic, Sept. 9–14, 2002*, Ed. by A. Wilson (European Space Agency, Noordwijk, 2002), Vol. 2, pp. 581–584.
5. I. De Moortel, "An overview of coronal seismology," Philos. Trans. R. Soc. London A **363**, 2743–2760 (2005).
6. I. De Moortel, "Propagating magnetohydrodynamics waves in coronal loops," Philos. Trans. R. Soc. London A **364**, 461 (2006).
7. I. De Moortel, "Longitudinal waves in coronal loops," Space Sci. Rev. **149**, 65–81 (2009).
8. I. De Moortel, A. W. Hood, J. Ireland, and R. W. Walsh, "Longitudinal intensity oscillations in coronal loops observed with trace. II. Discussion of measured parameters," Sol. Phys. **209**, 89–108 (2002).
9. I. De Moortel, J. Ireland, and R. W. Walsh, "Observation of oscillations in coronal loops," Astron. Astrophys. **355**, L23–L26 (2000).
10. I. De Moortel and V. M. Nakariakov, "Magnetohydrodynamic waves and coronal seismology: An overview of recent results," Philos. Trans. R. Soc. London A **370**, 3193–3216 (2012).
11. B. De Pontieu and S. W. McIntosh, "Quasi-periodic propagating signals in the solar corona: The signature of magneto-acoustic waves or high-velocity upflows," Astrophys. J. **722**, 1013–1029 (2010).
12. B. De Pontieu, S. W. McIntosh, V. H. Hansteen, and C. J. Schrijver, "Observing the roots of solar coronal heating in the chromosphere," Astrophys. J. **701**, L1–L6 (2009).
13. E. Devlen, D. Zengin Çamurdan, M. Yardımçı, and E. R. Pekünlü, "A new model for heating of the solar North Polar Coronal Hole," Mon. Not. R. Astron. Soc. **467**, 133–144 (2017).
14. N. Kitagawa, T. Yokoyama, S. Imada, and H. Hara, "Mode identification of MHD waves in an active region observed with Hinode/Eis," Astrophys. J. **721**, 744–749 (2010).
15. O. Kjeldseth-Moe and P. Brekke, "Time variability of active region loops observed with the coronal diagnostic spectrometer (CDS) on SOHO," Sol. Phys. **182**, 73–95 (1998).
16. S. Krishna Prasad, D. Banerjee, T. van Doorsselaere, and J. Singh, "Omnipresent long-period intensity oscillations in open coronal structures," Astron. Astrophys. **546**, A50 (2012).
17. S. G. Mamedov, Z. F. Shabanova, et al., "About heating of the solar corona," Azerb. Astron. J., No. 14, 62 (2014).
18. J. T. Mariska and K. Muglach, "Doppler-shift, intensity, and density oscillations observed with the extreme ultraviolet imaging spectrometer on Hinode," Astrophys. J. **713**, 573–583 (2010).
19. V. J. T. Mariska, H. P. Warren, D. R. Williams, and T. Watanabe, "Observations of Doppler shift oscillations with the EUV imaging spectrometer on Hinode," Astrophys. J. **681**, L41–L44 (2008).
20. M. P. McEwan and I. De Moortel, "Longitudinal intensity oscillations observed with TRACE: Evidence of fine-scale structure," Astron. Astrophys. **448**, 763–773 (2006).
21. S. W. McIntosh and B. De Pontieu, "High-speed transition region and coronal upflows in the Quiet Sun," Astrophys. J. **707**, 524–538 (2009).
22. V. M. Nakariakov and E. Verwichte, "Coronal waves and oscillations," Living Rev. Sol. Phys. **2**, 3 (2005).
23. L. Ofman, V. M. Nakariakov, and C. E. Deforest, "Slow magnetosonic waves in coronal plumes," Astrophys. J. **514**, 441–447 (1999).

24. L. Ofman and T. Wang, "Hot coronal loop oscillations observed by SUMER: Slow magnetosonic wave damping by thermal conduction," Astrophys. J. **580**, L85–L88 (2002).
25. E. O'Shea, D. Banerjee, and J. G. Doyle, "A statistical study of wave propagation in coronal holes," Astron. Astrophys. **463**, 713–725 (2007).
26. L. J. Porter, J. A. Klimchuk, and P. A. Sturrock, "The role of MHD waves in heating of the solar corona," Astrophys. J. **435**, 482–501 (1994).
27. T. Sakurai, K. Ichimoto, K. P. Raju, and J. Singh, "Spectroscopic observation of coronal waves," Sol. Phys. **209**, 265–286 (2002).
28. J. Threlfall, I. DeMoortel, S. W. McIntosh, and C. Bethge, "First comparison of wave observations from CoMP and AIA/SDO," Astron. Astrophys. **556**, A124 (2013).
29. E. Verwichte, M. Marsh, C. Foullon, T. Van Doorsselaere, I. De Moortel, A. W. Hood, and A. M. Nakariakov, "Periodic spectral line asymmetries in solar coronal structures from slow magnetoacoustic waves," Astrophys. J., Lett. **724**, L194–L198 (2010).
30. T. J. Wang, L. Ofman, J. M. Davila, and J. T. Mariska, "Hinode/EIS observations of propagating low-frequency slow magnetoacoustic waves in fan-like coronal loops," Astron. Astrophys. **503**, L25–L28 (2009).
31. T. J. Wang, S. K. Solanki, W. Curdt, D. E. Innes, and L. E. Dammasch, Oscillating hot loops observed by SUMER, in *Proc. SOHO 11 Symp. on From Solar Min to Max: Half a Solar Cycle with SOHO, Davos, Switzerland, Mar. 11–15, 2002* (European Space Agency, Noordwijk, 2002), paper id. ESASP.508.465W.
32. T. J. Wang, S. K. Solanki, D. E. Innes, W. Curdt, and E. Marsch, "Slow-mode standing waves observed by SUMER in hot coronal loops," Astron. Astrophys. **402**, L17–L20 (2003).

Translated by E. Petrova